Reducing Contact Resistance in Two-Dimensional-Material-Based Electrical Contacts by Roughness Engineering

Sneha Banerjee,[1] Liemao Cao,[2] Yee Sin Ang,[2,*] L.K. Ang,[2] and Peng Zhang[1,†]

[1] *Department of Electrical and Computer Engineering, Michigan State University, East Lansing, Michigan 48824-1226, USA*

[2] *Science, Math and Technology, Singapore University of Technology and Design (SUTD), 8 Somapah Road, Singapore 487372*

(Received 31 January 2020; revised manuscript received 6 May 2020; accepted 8 May 2020; published 9 June 2020)

The engineering of efficient electrical contacts to two-dimensional (2D) layered materials represents one of the major challenges in the development of industrial-grade 2D-material-based electronics and optoelectronics. In this paper, we present a computational study of the contact resistance and current-flow distribution for electrical contacts between 2D materials and three-dimensional (3D) metals and between different 2D materials. We develop models of the electrical contact resistance for 2D/2D and 2D/3D metal/semiconductor contact interfaces based on a self-consistent transmission-line model coupled with a thermionic charge-injection model for 2D materials and first-principles simulation by density-functional theory, which explicitly includes the variation of the electrostatic potential in the contact region. We compare the results of our self-consistent calculations with existing experimental work and obtain excellent agreement. It is found that the presence of contact interface roughness, in the form of fluctuating Schottky barrier heights in the contact region, can significantly reduce the contact resistance of MoS_2/metal Schottky 2D/3D contacts. Our findings suggest that roughness engineering may offer a possible paradigm for reducing the contact resistance of 2D-material-based electrical contacts.

DOI: 10.1103/PhysRevApplied.13.064021

I. INTRODUCTION

The undesirably large contact resistance between two-dimensional (2D) semiconductors and three-dimensional (3D) metallic electrodes represents one of the major obstacles to the development of practical 2D electronic and optoelectronic devices [1]. The engineering of better electrical contacts has become a key research objective in recent years. Extensive efforts have been made to improve current flow through contacts and to improve device performance in 2D-material-based devices [2–7]. Recent experimental breakthroughs have demonstrated that a van der Waals contact between a metal and a 2D semiconductor can significantly improve the quality of the electrical contact [8,9]. This advancement opens up exciting avenues for the exploration of how 2D/3D electrical contacts can be further improved. This leads to the need for a physical model that comprehensively includes both the material properties of 2D semiconductors and geometrical electrostatic effects in mixed-dimensional nanostructures; this topic has been studied only rarely in the literature thus far.

In this paper, we present a consistent model for calculating the contact resistance, which is important for realizing 2D-material-based electronics. This model includes elements that are absent in prior work, such as a consistent spatially dependent transmission-line model (TLM), an improved model for charge injection at a 2D electrical contact, and taking account of the effects of roughness. Our consistent model for 2D/3D or 2D/2D electrical contact resistances is based on coupling a recently developed thermionic charge-injection model for 2D materials [10] with a 2D TLM accounting for the varying specific contact resistivity along the contact length [11]. The latter has been recently applied to study nanoscale tunneling electrical contacts [11–13]. Here, using our self-consistent model for 2D-material-based contacts, profiles of the current and voltage distribution in the contact region and the total contact resistance are calculated for various input voltages, contact dimensions, material properties, and temperatures. It is found that one-dimensional (1D) models become less reliable when the Schottky barrier height (SBH) becomes smaller or when the applied voltage becomes larger, where our self-consistent model is expected to provide an improved evaluation of 2D-material-based electrical contacts. The results of our self-consistent calculations are compared with results obtained

*yeesin_ang@sutd.edu.sg
†pz@egr.msu.edu

 © 2020 American Physical Society

using the classic Richardson-Dushman (RD) thermionic law. We find that the RD law significantly underestimates the contact resistance and overestimates the contact current density for 2D-material-based contacts. We obtain excellent agreement when our numerically calculated results are compared with the reported experimental data [9,14,15].

Further, we incorporate the effects of interface roughness in 3D/2D electrical contacts into our 2D TLM model. Interface roughness can be introduced (or engineered) by substrate doping [16] and is inherently present due to the inevitable presence of interfacial defects during the fabrication process. The impact of surface roughness on the contact resistance of ohmic contacts has been studied previously [17–20]. Previous experiments have also demonstrated that substrate roughness can improve the mobility of 2D transition-metal dichalcogenides (TMDs) by several orders of magnitude [21]. In our model, the contact interface roughness is modeled as a fluctuating SBH [22] on the electrical contact. Using experimental device parameters for a Au/MoS_2 electrical contact [14], we show that the contact resistance of a 2D/3D Schottky contact can be reduced by more than one order of magnitude. The key finding that roughness can improve the quality of a 2D/3D electrical contact further highlights the technological importance of roughness engineering for improving device performance in 2D electronics and optoelectronics. Our findings provide a theoretical foundation for the modeling of contact resistance in 2D/2D and 2D/3D electrical contacts and establish a viable route towards the design of better electrical contacts to 2D materials using roughness engineering.

II. MODEL

Because of the reduced dimensionality and the exotic electronic properties of 2D materials, the physics of electron emission deviates significantly from that in traditional 3D materials [10,23–25]. The thermionic emission of charged carriers across a 2D-material-based metal/semiconductor Schottky contact [see Fig. 1(a) for a band diagram] is found to be universally governed by a simple current-temperature (J-T) scaling law [10], $\ln(J/T^{\beta}) = A - B/T$, where A and B are material- or device-dependent parameters, and $\beta = 1$ or 3/2 for a vertical or lateral Schottky contact, respectively. For 2D TMDs, such as atomically thin MoS_2, the thermionic emission is governed by

$$J_{\mathrm{th}}(V,T) = \frac{2e\Phi_{B0}k_B T}{\pi\tau\hbar^2 v_F^2}\left(1+\frac{k_B T}{\Phi_{B0}}\right)\exp\left(-\frac{\Phi_{B0}-\varepsilon_F}{k_B T}\right), \tag{1}$$

where Φ_{B0} is the intrinsic SBH, the Fermi velocity v_F is 1.1×10^6 m/s for MoS_2, ε_F is the Fermi level, and $\tau \approx (0.1–10)$ ps is the carrier-injection time, determined experimentally [26]. Equation (1) deviates significantly from the classic RD thermionic law for 3D materials, i.e., $\ln(J_{3D}/T^2) \propto 1/T$ [27]. The Shockley diode equation can thus be modified to

$$J_{2D}(V,T) = J_{\mathrm{th}}(V,T)\left[\exp\left(\frac{eV}{k_B T}\right)-1\right], \tag{2}$$

which is obtained based on the detailed-balance principle [27]. Equation (2) represents the generalized 2D Shockley diode equation for 2D electronic systems [10]. For comparison, the Shockley diode equation based on the 3D classic RD thermionic law is $J_{3D}(V,T) = J_{RD}(V,T)[\exp(eV/k_BT)-1]$, where $J_{RD}(V,T) = (4\pi m^* k_B^2 e/h^3)T^2\exp[-(\Phi_{B0}-\varepsilon_F)/k_BT]$ and $m^* = 0.54m_e$ [28], m_e being the mass of an electron.

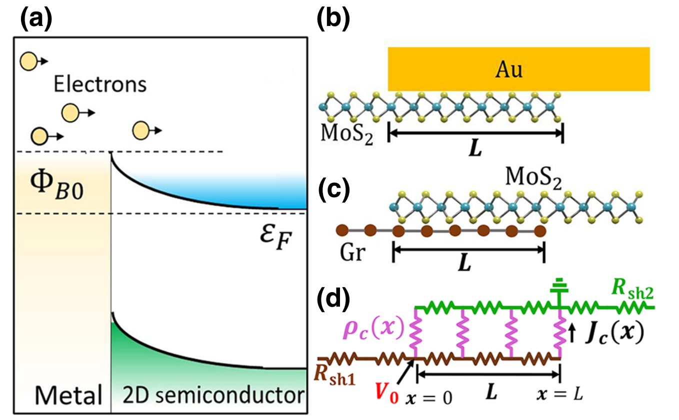

FIG. 1. (a) Band diagram of a 2D-semiconductor/3D-metal electrical contact. (b),(c) Parallel partially overlapping electrical contacts between (b) monolayer MoS_2 (2D semiconductor) and gold (3D metal), and (c) graphene (2D) and MoS_2 (2D). (d) Transmission-line model.

A 2D self-consistent TLM [11] is used to predict the profiles of the current and voltage distributions and the total contact resistance in nanoscale 2D/3D Schottky contacts. Consider a parallel contact between a 2D semiconductor and a 3D metal, or between two 2D nanosheets, as shown in Figs. 1(b) and 1(c). The dc equivalent-lump-circuit TLM [29–33] for these contacts can be constructed as shown in Fig. 1(d). A voltage V_0 is applied to the lower contact at $x=0$, the contact length is L, and the specific contact resistivity $\rho_c(x)$ is spatially dependent [11]. The governing equations can be written as

$$\frac{\partial I_1(x)}{\partial x} = -wJ_c(x), \quad \frac{\partial V_1(x)}{\partial x} = -\frac{I_1(x)R_{\mathrm{sh1}}}{w}, \tag{3a}$$

$$\frac{\partial I_2(x)}{\partial x} = wJ_c(x), \quad \frac{\partial V_2(x)}{\partial x} = -\frac{I_2(x)R_{\mathrm{sh2}}}{w}, \tag{3b}$$

where $I_1(x)$ and $I_2(x)$ represent the current flowing at x through the lower and upper contact members, respectively, $V_1(x)$ and $V_2(x)$ are the local voltages at x on

the lower and upper contact members, respectively, and w is the effective transverse dimension of the contacts. R_{sh1} and R_{sh2} are the sheet resistance of contact members 1 and 2, respectively. The sheet resistance of MoS_2 under a contact can be calculated semiempirically [14] as $R_{sh} = 1/ne\mu(T)$, where n is the 2D carrier density, with a typical value of 5×10^{12} cm^{-2}, e is the electron charge, and $\mu(T) = \mu_0(T/300)^{-1.6}$ is the temperature-dependent mobility. The spatially dependent specific contact resistivity $\rho_c(x)$ is calculated from the local voltage drop across the interface, $V(x) = V_1(x) - V_2(x)$, and the local contact current density $J_c(x)$ as $\rho_c(x) = V(x)/J_c(x)$. The boundary conditions for Eq. (3) are $V_1(x = 0) = V_0$, $I_2(x = 0) = 0$, $I_1(x = L) = 0$, $V_2(x = L) = 0$. Here, the contact current density is modeled by the thermionic injection mechanism of Eq. (2), i.e., $J_c(x) = J_{2D}[V(x), T]$. The contact resistance can be calculated by self-consistently solving Eqs. (1)–(3) to obtain

$$R_c = \frac{V_0 w}{I_{tot}}, \tag{4}$$

where I_{tot} is the total current in the circuit, which is uniquely determined by the boundary conditions of Eq. (3) [11]. The details of the procedure for self-consistently solving the coupled Eqs. (1)–(3) can be found in Ref. [11]. It is important to note that the TLM is only a simplified approximation to a 2D/3D electrical contact, where accurate evaluation of current crowding and the fringing fields near the corners of the contact in the 3D metal requires field-solution methods [34–36].

III. RESULTS AND DISCUSSION

In Fig. 2, we show self-consistent calculations of the voltage drop $V(x)$, the injection current density $J_c(x)$, and the contact resistivity $\rho_c(x)$ across the contact region for a fixed bias voltage $V_0 = 0.1$ V with different interface charge-injection times τ, for a MoS_2/Au contact using the experimentally determined device parameters reported previously [14]. In Fig. 2(a), it is found that $V(x)$ is nonuniform over the contact length. The variation of $V(x)$ increases with decreasing charge-injection time, which indicates a stronger current-crowding effect in the 2D/3D interface for a higher carrier-injection efficiency, as shown in Fig. 2(b). This is consistent with previous studies, which show that the current-crowding effect increases with more conductive contact interfaces [31,35,36]. The spatially dependent contact resistivity is more evenly distributed across the contact region for contacts with a longer injection time [Fig. 2(c)].

In Figs. 3(a) and 3(b), the contact resistance R_c calculated from Eqs. (1)–(3) is shown as a function of the bias voltage for two different SBHs for the 2D/3D contact in Fig. 1(b). The 2D/3D contact exhibits a transition from a Schottky contact characteristic, in which R_c increases with decreasing temperature for $V_0 < \Phi_B$, to an ohmic contact characteristic, in which R_c increases with increasing temperature for $V_0 > \Phi_B$. Such a transition is due to the offset of the SBH caused by the external bias voltage. In Figs. 3(c) and 3(d), the temperature dependence of R_c further confirms the Schottky-to-ohmic transition at $V_0 \sim \Phi_B$ observed in Figs. 3(a) and 3(b), which is also consistent with experimental results [14].

In Fig. 4, $V(x)$, $J_c(x)$, and $\rho_c(x)$ for a MoS_2/Ag contact are shown for varying contact length L. The current

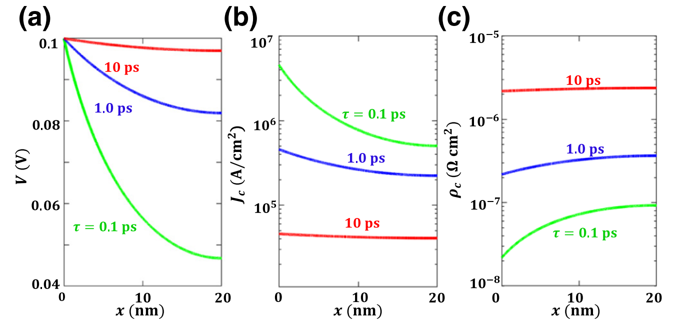

FIG. 2. (a) Voltage drop $V(x)$, (b) current density $J_c(x)$, and (c) specific contact resistivity $\rho_c(x)$ across the contact interface for a contact between monolayer MoS_2 (2D semiconductor) and gold (3D metal) for different carrier-injection times τ with a fixed applied voltage $V_0 = 0.1$ V and a contact length $L = 20$ nm. Here, $R_{sh1}(MoS_2) = 35\,714\ \Omega/\square$, $R_{sh2}(\text{Au}) = 4.4\ \Omega/\square$, $\Phi_B = 0.1$ eV , $\varepsilon_F = 0.8$ eV, and $T = 300$ K.

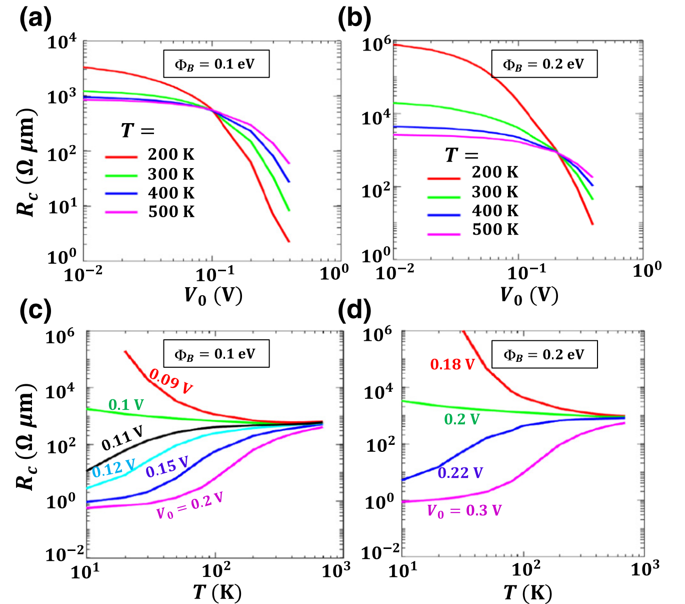

FIG. 3. (a),(b) Contact resistance R_c as a function of applied voltage V_0 for different values of T, for (a) $\Phi_B = 0.1$ eV and (b) $\Phi_B = 0.2$ eV . (c),(d) R_c as a function of T for different values of V_0, for (c) $\Phi_B = 0.1$ eV and (d) $\Phi_B = 0.2$ eV . Here, the contact is between monolayer MoS_2 and Au, with $\tau = 0.1$ ps and $L = 50$ nm.

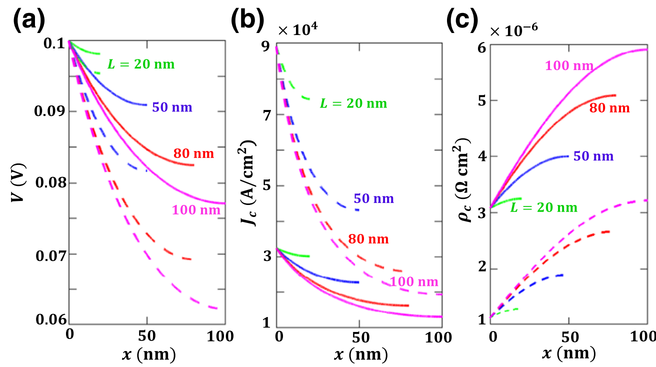

FIG. 4. (a) Voltage drop $V(x)$, (b) current density $J_c(x)$, and (c) specific contact resistivity $\rho_c(x)$ across the contact interface for MoS_2/Ag contacts with different contact lengths L and fixed applied voltage $V_0 = 0.1$ V. The solid lines are for self-consistent calculations of model A, and the dashed lines for model C. See text for details. Here, $\tau = 0.1$ ps, $R_{sh1}(MoS_2) = 30\,000\ \Omega/\square$, $R_{sh2}(\mathrm{Ag}) = 3.18\ \Omega/\square$, $\varepsilon_F = 0.249$ eV, $\Phi_B = 0.212$ eV, and $T = 300$ K.

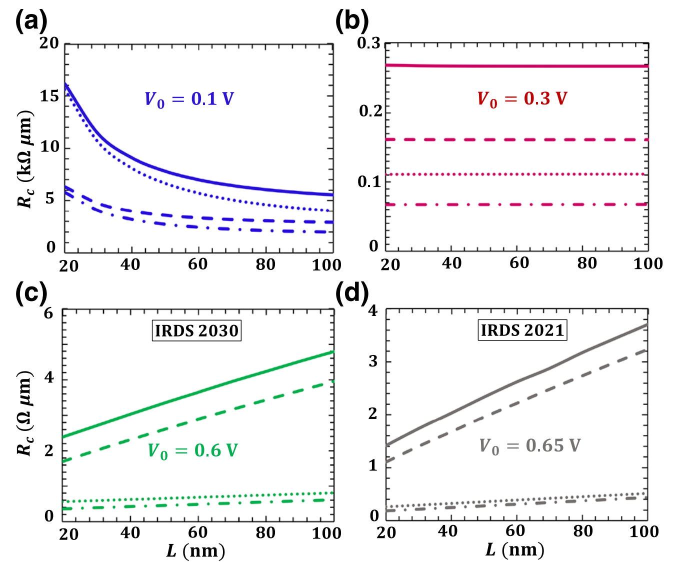

FIG. 5. Contact resistance R_c for MoS_2/Ag contacts as a function of contact length L for different applied biases V_0= (a) 0.1 V, (b) 0.3 V, (c) 0.60 V, and (d) 0.65 V. The two bias voltages in (c) and (d) are the required industry standards according to the International Roadmap of Devices and Systems [37] for the years 2030 and 2021, respectively. The solid lines are for self-consistent calculations of model A, the dotted lines for model B, the dashed lines for model C, and the dash-dotted lines for model D. See text for details. Here, $\tau = 0.1$ ps, $R_{sh1}(MoS_2) = 30\,000\ \Omega/\square$, $R_{sh2}(\mathrm{Ag}) = 3.18\ \Omega/\square$, $\varepsilon_F = 0.249$ eV, $\Phi_B = 0.212$ eV, and $T = 300$ K.

crowding is strongly amplified in the case of a long contact length, because the applied voltage is distributed over a longer resistive network (Fig. 1), resulting in an increased interface contact resistivity due to the voltage-dependent Schottky barrier. The influence of L on R_c is shown in Fig. 5 for different applied voltages. In Figs. 4 and 5, we calculate the results using four different approaches: model A, self-consistent calculations using Eqs. (1)–(3) (solid lines); model B, an analytical solution [11] of Eq. (3) assuming constant ρ_c, calculated using a fixed $V = V_0$ in Eq. (2) (dotted lines); model C, calculations using Eq. (3) with the 3D Richardson-Dushman injection model for $J_{3D}(V, T)$ (dashed lines); and model D, an analytical solution [11] of Eq. (3) assuming constant ρ_c, calculated using a fixed $V = V_0$ in the Richardson-Dushman injection model for $J_{3D}(V, T)$ (dash-dotted lines). It is found that, for 2D/3D contacts, the classic Richardson-Dushman injection model significantly underestimates the contact resistance and overestimates the contact current density. We also find that, as V_0 increases, the analytical solutions [11] of the TLM in Eq. (3) with constant ρ_c calculated using $V = V_0$ in the charge-injection model, which is almost always used in the literature [9,14,15], becomes less reliable; our proposed self-consistent model may be used to obtain a more accurate evaluation of such contacts. This aspect is particularly important in the development of industrial-grade field-effect transistors based on 2D semiconductors. According to the International Roadmap of Devices and Systems (IRDS) [37], the required industry-standard bias voltage is 0.65 V and 0.60 V for the years 2021 and 2030, respectively. At these bias-voltage values, we find that both the analytical model with both constant ρ_c and the Richardson-Dushman thermionic injection model severely underestimate the contact resistance by at least 75% (model B), 30% (model C), and 83% (model D) when compared with our self-consistent model combined with the 2D thermionic charge-injection theory (model A), over a wide range of contact lengths L from 20 to 100 nm.

Density-functional theory (DFT) has been extensively employed to understand the interfacial contact physics in 2D-material-based heterostructure devices [5–7]. Based on DFT simulation results for a MoS_2/metal heterostructure [38], we calculate the bias dependence of the contact resistance of a MoS_2/M interface [Fig. 6(a)], where M = Ag, Au, Ni. It is found that the contact resistance R_c is almost independent of the bias voltage V_0 for $V_0 < 0.05$ V in all three cases. However, for $V_0 > 0.05$ V, R_c decreases sharply with increasing V_0. This is because the thermionic-emission-dependent specific contact resistivity ρ_c decreases nonlinearly with the bias voltage for such contacts. Further, we perform DFT calculations for various graphene-based 2D/2D electrical contacts using the Vienna *ab initio* simulation package (VASP). The projector-augmented wave method is used to describe the electron interaction. The exchange and correlation potentials are treated using the Perdew-Burke-Ernzerhof generalized gradient approximation. All the lattice mismatches are smaller than 1% in our calculations. The calculated interfacial Schottky barrier height, Fermi level, and interlayer

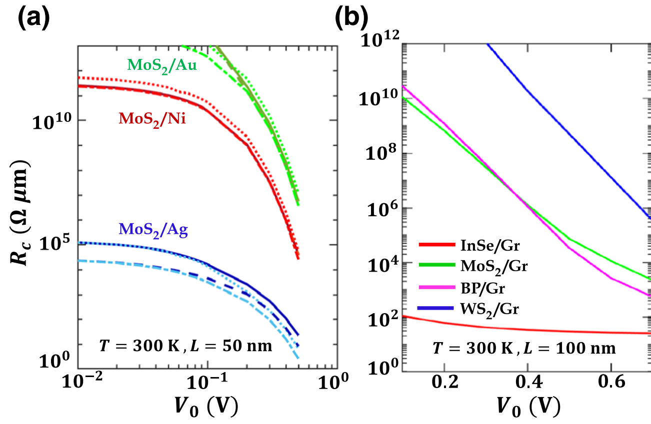

FIG. 6. R_c as a function of applied voltage V_0 for different (a) 2D/3D and (b) graphene (Gr)-based 2D/2D Schottky contacts. BP, black phosphorus. In (a), $R_{sh}(\mathrm{Au}) = 4.4\ \Omega/\square$, $R_{sh}(\mathrm{Ag}) = 3.18\ \Omega/\square$, and $R_{sh}(\mathrm{Ni}) = 13.8\ \Omega/\square$; the values of ε_F and Φ_B for the three contacts are taken from Ref. [38]. The solid lines are for self-consistent calculations of model A, the dotted lines for model B, the dashed lines for model C, and the dash-dotted lines for model D. See text for details. In (b), $\tau = 0.1$ ps, $R_{sh}(\mathrm{Gr}) = 156.25\ \Omega/\square$, $R_{sh}(\mathrm{InSe}) = 6.25\ \mathrm{k}\Omega/\square$, $R_{sh1}(\mathrm{MoS_2}) = 62.5\ \mathrm{k}\Omega/\square$, $R_{sh}(\mathrm{BP}) = 6.25\ \mathrm{k}\Omega/\square$, $R_{sh}(\mathrm{WS_2}) = 12.860\ \mathrm{k}\Omega/\square$, and $v_F = 1.1 \times 10^6$ m/s; the values of ε_F and Φ_B for the four contacts are taken from Table I.

separation of the 2D/2D heterostructures are summarized in Table I. Based on the DFT simulated heterostructure parameters in Table I, the self-consistent model is employed to calculate the resistance of graphene-based 2D/2D electrical contacts. Figure 6(b) suggests that a 2D semiconductor with a higher sheet conductivity produces a lower contact resistance when contacted by graphene.

Next, we compare our self-consistent model with existing experimental work (Figs. 7 and 8) for various 2D carrier densities n, temperatures, and MoS_2-metal interfaces. With suitable values of V_0 and τ, the results from our self-consistent model are in excellent agreement with the experimental data. Figure 7 shows that for a given temperature T, the contact resistance R_c decreases with increasing n, as has been reported previously [9,14,15]. It is evident that the calculations based on our self-consistent model provide a much better fit to the experimental data for 2D-material-metal electrical contacts than models based on the 3D Richardson-Dushman injection law.

Figure 8 shows a comparison of our self-consistent model with experimental results for R_c as a function of

TABLE I. Material parameters of graphene-based 2D/2D electrical contacts calculated using DFT simulation.

	MoS_2/Gr	WS_2/Gr	InSe/Gr	BP/Gr
Φ_B (eV)	0.621	0.911	0.058	0.643
ε_F (eV)	0.608	0.502	0.671	0.1335
d (Å)	3.37	3.36	3.46	3.55

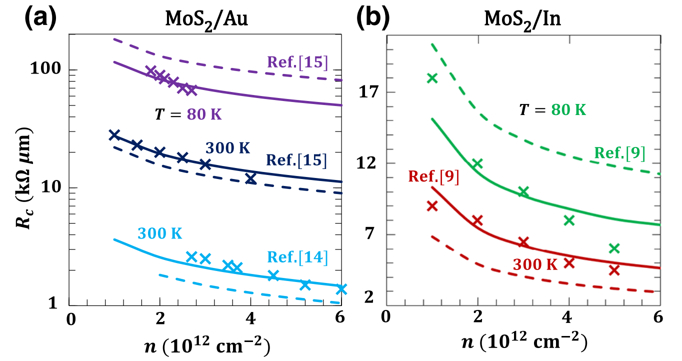

FIG. 7. R_c as a function of 2D carrier density n at different temperatures for (a) MoS_2/Au contacts and (b) MoS_2/In contacts. The cross symbols are from experiments [15,9,14], the solid lines are from our self-consistent model using Eqs. (1)–(3), model A, and the dashed lines are from Eq. (3) with the Richardson-Dushman injection model, model C. In the calculation, we use $R_{sh}(\mathrm{Au}) = 2.2\ \Omega/\square$, $R_{sh}(\mathrm{In}) = 8.37\ \Omega/\square$, and $\mu_0 = 20\ \mathrm{cm^2\,V^{-1}\,S^{-1}}$ for MoS_2/Au contacts [14], and $\mu_0 = 170\ \mathrm{cm^2\,V^{-1}\,S^{-1}}$ for MoS_2/In contacts [9]. The parameters $\varepsilon_F = 0.077$ eV [38], 0.6 eV [9], and 0.5 eV, $\Phi_B = 0.763$ eV [38], 0.3 eV [9], 0.15 eV [14], and $\tau = 0.1$, 0.15, and 0.1 ps are used to fit the experimental results in Refs. [15,9,14], respectively. In the different cases shown, from top to bottom, input voltages $V_0 = 0.731, 0.7, 0.1$ V are used in (a) and $V_0 = 0.271, 0.17$ V are used in (b). $L = 500$ nm [14] is assumed in all cases.

the temperature T for different values of n, for MoS_2/metal contacts. In all cases, our self-consistent calculation based on model A (solid lines) provides a much better fit to the experimental data (symbols) than do the existing models [14] (dashed lines). The three red lines in Fig. 8(a), with input voltages $V_0 = 0.635$, 0.64, and 0.645 V from top to bottom, show that the increasing (ohmic characteristic) or decreasing (Schottky characteristic) trend of R_c with temperature depends very sensitively on the input voltage V_0 applied to the contact, which is also evident in Fig. 3. This voltage dependence of the contact resistance has not been emphasized and is generally missing in previous work [9,14,15]. Our model suggests that the input voltage must be specified in order to give a meaningful characterization of the contact resistance for a given 2D-material-metal contact.

Further, we model the effect of interface roughness in a 2D/3D electrical contact by including a SBH fluctuation term, i.e., $\Phi_B \rightarrow \Phi_B + \Delta\Phi_B$, where $\Delta\Phi_B$ is calculated by assuming that the SBH fluctuations follow a Gaussian distribution. The fluctuations of the SBH, injection current, and contact resistivity are shown in Figs. 9(a), 9(b), and 9(c), respectively. As shown in Fig. 9(d), the variation in the SBH has a dramatic effect on the contact resistance. In general, R_c is reduced significantly in the presence of roughness. This reduction is particularly effective for MoS_2/Au contacts with a large SBH (e.g., 0.3 eV). Such a roughness-induced contact-resistance reduction is

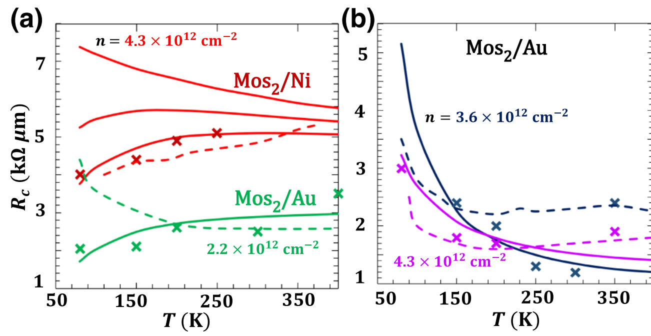

FIG. 8. R_c as a function of temperature T with (a) an increasing trend, and (b) a decreasing trend, for MoS_2/metal contacts with different values of n. The cross symbols are from experiments [14], the solid lines are from our self-consistent model A, and the dashed lines are taken from the model calculations in Ref. [14]. In the calculation, we use $R_{\rm sh}(\mathrm{Au}) = 2.2\ \Omega/\square$ and $R_{\rm sh}(\mathrm{Ni}) = 13.8\ \Omega/\square$. The parameters $\varepsilon_F = 0.588$ eV, $\Phi_B = 0.633$ eV [38] and $\varepsilon_F = 0.5$ eV, $\Phi_B = 0.150$ eV [14] are used for MoS_2/Ni and MoS_2/Au contacts, respectively. In (a), for the three solid red lines, from top to bottom, $V_0 = 0.635, 0.64, 0.645$ V, respectively, all with $\tau = 0.45$ ps; for the green solid line, $V_0 = 0.165$ V and $\tau = 0.7$ ps. In (b), $V_0 = 0.13, 0.141$ V and $\tau = 0.1, 0.2$ ps for the blue and purple solid lines, respectively. Values of $\mu_0 = 20$ cm^2 V^{-1} S^{-1} [14] and $L = 500$ nm [14] are assumed in all cases.

reminiscent of the previously reported mobility enhancement in 2D TMDs due to the presence of a crested rough substrate [21]. Thus, the findings in Fig. 9(d) suggest that roughness not only improves the mobility but also decreases the contact resistance with a 3D metal. A reduction of the contact resistance with interface roughness is also achieved in 1D electrical contacts, i.e., when both contact members [see Figs. 1(b) and 1(c)] have constant voltages applied uniformly across the contact region (not shown).

The reduction in contact resistance due to fluctuations of the interface resistance can be easily understood from general circuit theory. Consider a rough resistive interface between two conductors. Because of fluctuations of the conductivity along the interface, there will be local regions of highly conductive spots, whose resistance can be much smaller than that of a uniform interface. Such a resistive interface may be considered as a set of equivalent elementary resistors connected in parallel along the interface between the two contacting members; the total resistance of this interface is $R_{\rm total} = 1/[(1/R_1) + (1/R_2) + \ldots + (1/R_N)] \sim \{R_i\}_{\rm minimum}$, which is determined by the smallest resistor in the parallel connection, i.e., the equivalent resistor at a highly conductive spot. As a result, this leads to a reduced overall interface resistance compared with a uniform interface. Note that the interface "roughness" represents the variation or fluctuations in the conductivity over the interface (e.g., induced by doping, SBH, etc.) and needs not be a physical roughness. Similar benefits of

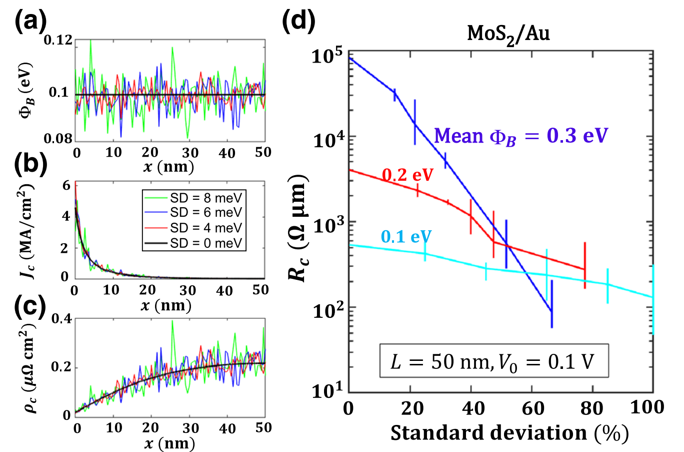

FIG. 9. (a) Roughness of Schottky barrier height Φ_B, (b) resulting current density $J_c(x)$, and (c) specific contact resistivity $\rho_c(x)$ across the contact interface for a monolayer-MoS_2/Au 2D/3D contact for different values of standard deviation (SD). (d) Contact resistance R_c as a function of surface roughness (standard deviation/Φ_B) for different mean values of Φ_B. Here, the applied voltage $V_0 = 0.1$ V, and the contact length $L = 50$ nm.

surface roughness are found in the form of a decrease in the contact resistance in organic transistors [18] and an increase in the mobility of charge carriers in organic and 2D transistors [18,21].

IV. CONCLUSIONS

In summary, a self-consistent transmission-line model to quantify and model the current distribution and contact resistance in 2D-material-based contacts is constructed and validated against existing experimental work. It is found that interface roughness can significantly reduce the resistance of 2D/3D electrical contacts. Our findings provide a theoretical foundation for the modeling of 2D/2D and 3D/2D electrical contacts and, further, reveal a possible route towards efficient electrical contacts to 2D materials through roughness engineering.

ACKNOWLEDGMENTS

This work is supported by an Air Force Office of Scientific Research (AFOSR) YIP Award (Grant No. FA9550-18-1-0061), an A*STAR AME IRG Grant (Grant No. A1783c0011), and a Singapore MOE Tier 2 Grant (Grant No. 2018-T2-1-007).

[1] A. Allain, J. Kang, K. Banerjee, and A. Kis, Electrical contacts to two-dimensional semiconductors, Nat Mater. 14, 1195 (2015).

[2] S. Das, H.-Y. Chen, A. V. Penumatcha, and J. Appenzeller, High performance multilayer MoS_2 transistors with scandium contacts, Nano Lett. 13, 100 (2013).

[3] H.-Y. Chang, S. Yang, J. Lee, L. Tao, W.-S. Hwang, D. Jena, N. Lu, and D. Akinwande, High-performance, highly bendable MoS_2 transistors with high-k dielectrics for flexible low-power systems, ACS Nano **7**, 5446 (2013).

[4] Y. Xu, C. Cheng, S. Du, J. Yang, B. Yu, J. Luo, W. Yin, E. Li, S. Dong, P. Ye, and X. Duan, Contacts between Two- and three-dimensional materials: Ohmic, Schottky, and p–n heterojunctions, ACS Nano **10**, 4895 (2016).

[5] X. Ding, S. Zhang, M. Zhao, Y. Xiang, K. H. L. Zhang, X. Zu, S. Li, and L. Qiao, Nbs_2: A Promising p-Type Ohmic Contact for Two-Dimensional Materials, Phys. Rev. Appl. **12**, 064061 (2019).

[6] Y. Liu, P. Stradins, and S.-H. Wei, Van der waals metal-semiconductor junction: Weak Fermi level pinning enables effective tuning of schottky barrier, Sci. Adv. **2**, e1600069 (2016).

[7] F. Zhang, W. Li, Y. Ma, Y. Tang, and X. Dai, Tuning the schottky contacts at the graphene/WS_2 interface by electric field, RSC Adv. **7**, 29350 (2017).

[8] Y. Liu, J. Guo, E. Zhu, L. Liao, S.-J. Lee, M. Ding, I. Shakir, V. Gambin, Y. Huang, and X. Duan, Approaching the Schottky-Mott limit in van der Waals metal-semiconductor junctions, Nature **557**, 696 (2018).

[9] Y. Wang, J. C. Kim, R. J. Wu, J. Martinez, X. Song, J. Yang, F. Zhao, A. Mkhoyan, H. Y. Jeong, and M. Chhowalla, Van der Waals contacts between three-dimensional metals and two-dimensional semiconductors, Nature **568**, 70 (2019).

[10] Y. S. Ang, H. Y. Yang, and L. K. Ang, Universal Scaling Laws in Schottky Heterostructures Based on Two-Dimensional Materials, Phys. Rev. Lett. **121**, 056802 (2018).

[11] S. Banerjee, J. Luginsland, and P. Zhang, A Two dimensional tunneling resistance transmission line model for nanoscale parallel electrical contacts, Sci. Rep. **9**, 14484 (2019).

[12] P. Zhang, Scaling for quantum tunneling current in nano- and subnano-scale plasmonic junctions, Sci. Rep. **5**, 9826 (2015).

[13] S. Banerjee and P. Zhang, A generalized self-consistent model for quantum tunneling current in dissimilar metal-insulator-metal junction, AIP Adv. **9**, 085302 (2019).

[14] C. D. English, G. Shine, V. E. Dorgan, K. C. Saraswat, and E. Pop, Improved contacts to MoS_2 transistors by ultra-high vacuum metal deposition, Nano Lett. **16**, 3824 (2016).

[15] K. K. H. Smithe, C. D. English, S. V. Suryavanshi, and E. Pop, Intrinsic electrical transport and performance projections of synthetic monolayer MoS_2 devices, 2D Mater. **4**, 011009 (2016).

[16] N. Kaushik, A. Nipane, F. Basheer, S. Dubey, S. Grover, M. M. Deshmukh, and S. Lodha, Schottky barrier heights for Au and Pd contacts to MoS_2, Appl. Phys. Lett. **105**, 113505 (2014).

[17] F. Pennec, D. Peyrou, D. Leray, P. Pons, R. Plana, and F. Courtade, Impact of The surface roughness description on the electrical contact resistance of ohmic switches under low actuation forces, IEEE Trans. Compon. Packag. Technol. **2**, 85 (2012).

[18] Z. A. Lamport, K. J. Barth, H. Lee, E. Gann, S. Engmann, H. Chen, M. Guthold, I. McCulloch, J. E. Anthony, L. J. Richter, D. M. DeLongchamp, and O. D. Jurchescu, A simple and robust approach to reducing contact resistance in organic transistors, Nat. Commun. **9**, 5130 (2018).

[19] Y. Gao, L. Liu, W. Ta, and J. Song, Effect of surfaces similarity on contact resistance of fractal rough surfaces under cyclic loading, AIP Adv. **8**, 035319 (2018).

[20] P. Zhang, PhD Thesis, the University of Michigan, Ann Arbor, 2012.

[21] T. Liu, S. Liu, K.-H. Tu, H. Schmidt, L. Chu, D. Xiang, J. Martin, G. Eda, C. A. Ross, and S. Garaj, Crested two-dimensional transistors, Nat. Nanotechnol. **14**, 223 (2019).

[22] S.-J. Liang, W. Hu, A. Di Bartolomeo, S. Adam, and L. K. Ang, in *2016 IEEE International Electron Devices Meeting (IEDM)* (2016), pp. 14.4.1–14.4.4.

[23] Y. S. Ang and L. K. Ang, Current-Temperature Scaling for a Schottky Interface with Nonparabolic Energy Dispersion, Phys. Rev. Appl. **6**, 034013 (2016).

[24] Y. S. Ang, Y. Chen, C. Tan, and L. K. Ang, Generalized High-Energy Thermionic Electron Injection at Graphene Interface, Phys. Rev. Appl. **12**, 014057 (2019).

[25] Y. S. Ang, S.-J. Liang, and L. K. Ang, Theoretical modeling of electron emission from graphene, MRS Bull. **42**, 505 (2017).

[26] D. Sinha and J. U. Lee, Ideal graphene/silicon schottky junction diodes, Nano Lett. **14**, 4660 (2014).

[27] M. Sze and K. K. Ng, *Physics of Semiconductor Devices* (John Wiley & Sons, Hoboken, New Jersey, 2006).

[28] E. S. Kadantsev and P. Hawrylak, Electronic structure of a single MoS_2 monolayer, Solid State Commun. **152**, 909 (2012).

[29] D. K. Schroder, *Semiconductor Material and Device Characterization* (Wiley-Blackwell, Hoboken, New Jersey, 1998).

[30] H. H. Berger, Contact resistance and contact resistivity, J. Electrochem. Soc. **119**, 507 (1972).

[31] P. Zhang and Y. Y. Lau, An exact field solution of contact resistance and comparison with the transmission line model, Appl. Phys. Lett. **104**, 204102 (2014).

[32] H. Murrmann and D. Widmann, Current crowding on metal contacts to planar devices, IEEE Trans. Electron. Devices **16**, 1022 (1969).

[33] S. Banerjee, P. Wong, and P. Zhang, Contact resistance and current crowding in tunneling type circular nano-contacts, J. Phys. D: Appl. Phys. accepted, (2020).

[34] P. Zhang, Y. Y. Lau, and R. M. Gilgenbach, Minimization of thin film contact resistance, Appl. Phys. Lett. **97**, 204103 (2010).

[35] P. Zhang, D. M. H. Hung, and Y. Y. Lau, Current flow in a 3-terminal thin film contact with dissimilar materials and general geometric aspect ratios, J. Phys. D: Appl. Phys. **46**, 065502 (2013).

[36] P. Zhang, Y. Y. Lau, and R. M. Gilgenbach, Analysis of current crowding in thin film contacts from exact field solution, J. Phys. D: Appl. Phys. **48**, 475501 (2015).

[37] International Roadmap for Devices and Systems (IRDS™) 2017, IEEE, https://irds.ieee.org/editions/2017.

[38] H. Zhong, R. Quhe, Y. Wang, Z. Ni, M. Ye, Z. Song, Y. Pan, J. Yang, L. Yang, M. Lei, J. Shi, and J. Lu, Interfacial properties of monolayer and bilayer MoS_2 contacts with metals: Beyond the energy band calculations, Sci. Rep. **6**, 21786 (2016).